energies

MDPI

Article

A Novel Protection Scheme for Solar Photovoltaic Generator Connected Networks Using Hybrid Harmony Search Algorithm-Bollinger Bands Approach

Vipul N. Rajput [1], Kartik S. Pandya [2], Junhee Hong [3] and Zong Woo Geem [3,*]

1 Department of Electrical Engineering, Dr. Jivraj Mehta Institute of Technology, Anand 388340, India; vipulrajput16986@gmail.com
2 Department of Electrical Engineering, Charotar University of Science and Technology, Changa 388421, India; kartikpandya.ee@charusat.ac.in
3 Department of Energy IT, Gachon University, Seongnam 13120, Korea; hongpa@gachon.ac.kr
* Correspondence: geem@gachon.ac.kr; Tel.: +82-31-750-5586

Received: 26 April 2020; Accepted: 11 May 2020; Published: 13 May 2020

Abstract: This paper introduces a new protection system for solar photovoltaic generator (SPVG)-connected networks. The system is a combination of voltage-restrained overcurrent relays (VROCRs) and directional overcurrent relays (DOCRs). The DOCRs are implemented to sense high fault current on the grid side, and VROCRs are deployed to sense low fault current supplied by the SPVG. Furthermore, a novel challenge for the optimal coordination of DOCRs-DOCRs and DOCRs-VROCRs is formulated. Due to the inclusion of additional constraints of VROCR, the relay coordination problem becomes more complicated. To solve this complex problem, a hybrid Harmony Search Algorithm-Bollinger Bands (HSA-BB) method is proposed. Also, the lower and upper bands in BB are dynamically adjusted with the generation number to assist the HSA in the exploration and exploitation stages. The proposed method is implemented on three different SPVG-connected networks. To exhibit the effectiveness of the proposed method, the obtained results are compared with the genetic algorithm (GA), particle swarm optimization (PSO), cuckoo search algorithm (CSA), HSA and hybrid GA-nonlinear programming (GA-NLP) method. Also, the superiority of the proposed method is evaluated using descriptive and nonparametric statistical tests.

Keywords: Harmony Search Algorithm; Bollinger Bands; directional overcurrent relay; voltage restrained overcurrent relay; optimum relay coordination; solar photovoltaic generator; statistical test; power system protection; artificial intelligence; microgrid protection

1. Introduction

As fossil fuel reserves are depleting, the price and related environmental concerns strongly encourage the use of renewable energies [1–3]. The solar photovoltaic generator (SPVG) is one of the premier alternatives to fossil fuels that generates AC from DC power by using inverters. However, the response of SPVG to grid faults is more or less controllable by the power electronics used in an inverter system [1]. Thus, this difference has to be considered when designing a protective system for SPVG-connected networks [4].

In a network without distributed generators (DGs), directional overcurrent relays (DOCRs) are a suitable choice for the protection systems because of their ease in functionality and cost-effectiveness. In the last decade, a range of evolutionary algorithms and their hybrid approaches have become recognized as a means for solving the coordination problem of DOCRs [5–11].

Overcurrent-based protective systems have shown their effectiveness for conventional power systems, but this has been changing gradually due to the rising inclusion of DGs and power electronic devices. Inverters used in SPVG, because of the low thermal overload capability, are actively current limited and have a small current contribution (1.2 to 1.5 times the normal current in the grid fault condition) [1,12]. As a result, the overcurrent protection for the grid-connected configuration appears to take more fault clearing time. The responsive characteristics of overcurrent relay are essential for addressing this, but they are not endurable for a protection scheme. Protecting the inverter-dominated DGs such as SPVGs is, therefore, a challenging technical issue.

To address this issue, an inverse time admittance (ITA) relay, which is independent of current, has been used for an inverter-interfaced DGs (IIDGs)-connected network to sense and remove faulty section under low or changing fault current levels [13]. Major concerns for applications of ITA relay are the measurements of the admittance for short lines, fault resistance, and harmonic and transient behavior of current.

In [14], the frequency-based protection scheme is shown by using anti-islanding frequency relays. A significant issue with this scheme is that it is not practical to assume that all relays can be replaced [15].

Fault current limiter (FCL), another advanced technique, is used to limit the fault current supplied by DGs during grid fault. It restores the original settings of DOCRs [16–18]. However, the mutual influence of DGs makes it problematic, considering the impedance value of the FCL for a high level of DG penetration. The switching losses are also a major issue with this approach [16,19]. Hence, this approach is not suitable for increasing installations of SPVG with maximum capacities.

As IIDGs are a good resource of harmonics, a protection system based on the harmonic injection is proposed [20]. In this scheme, harmonics are injected into the network during a fault. Protection relays are used to observe and disconnect the inverter if the total harmonic distortion of terminal voltage exceeds the threshold value during a fault. This technique may fail when the numbers of dynamic loads are present. Furthermore, protection schemes with an advance communication infrastructure—e.g., adaptive relaying [21], communication-assisted digital relays [22], a phasor measurement units-assisted integrated impedance angle based scheme [23], or a microgrid central protection unit [15]—can effectively solve protection issues in an SPVG-connected network. However, the cost involved in their communication infrastructure and for updating the existing protection devices cannot justify these choices. Also, the risk of failing communication channels and threats of cybersecurity are an issue for employing these protective systems [24].

The different protection schemes [25,26] are used in a micro-grid, having synchronous and inverter-based DGs. The problems of communication cost and its failure, unbalanced loads, transients during connection and disconnections of DGs are associated with these schemes. While using energy storage devices such as the flywheel and batteries, the fault current can be increased at desired levels, letting the overcurrent relays to work traditionally [27,28]. Conversely, this method requires a significant investment and correct maintenance for safe operation. Recently, non-standard characteristics-based protection schemes were suggested for microgrid protection [29–31]. These types of characteristics provide flexibility in the operation of relays, but the complexity of the mathematical expressions and extra controlling parameters are challenging issues [32]. Overall, these solutions are not adequate for increasing installations of SPVG with maximum capacity.

As discussed in [33,34], the inverters and the point of common coupling (PCC) of the grid-connected SPVG system are perturbed by grid fault condition. It is rare but possible that the damage of SPVG is caused by an accident in the distribution network where most SPVGs are connected. Most damages resulting from faults in the distribution network can be protected by the inverters installed in the SPVG. However, if this protection fails, the central inverter installed in the SPVG will be damaged.

If the inverter installed in the SPVG (central inverter or string inverter) fails, the generation of the entire SPVG is stopped. For example, in South Korea, if an inverter of 1 MW SPVG fails, power generation stops for a period of two to four weeks, and the expected generation revenue during that period (in case of 4.8 h/day generation) is 67.2 to 134.4 MWh of electricity [3,35]. In order to

connect a SPVG system to the grid, a set of devices of protection are provided at PCC. This protection system performs the appropriate functions to prevent the SPVG feeds the network in case of abnormal values of current, voltage and frequency.

This paper:

- demonstrates that to develop a reliable protection scheme for SPVG-connected networks, voltage-restrained overcurrent relays (VROCRs) are deployed to sense a low fault current on the SPVG side, whereas DOCRs are used to operate with a high fault current on the grid side. VROCRs can sense a low fault current by providing the set overcurrent operating value in proportion to the applied input voltage. Also, VROCRs helps to maintain grid stability because they can avoid unnecessary isolations of SPVG networks against short-term disturbances such as voltage dips due to the fault cleared by DOCRs.
- formulates a new problem of optimum coordination of DOCRs-DOCRs and DOCRs-VROCRs in SPVG-connected networks.
- hybridizes the Harmony Search Algorithm (HSA) with the Bollinger Bands (BB) approach for accelerating a local search and improving the convergence and accuracy of the results. The BB method is also modified to support HSA in exploration and exploitation.
- estimates the performance of the proposed hybrid approach by applying over three case studies. The outcomes in terms of the total operating time, violations in constraints, and convergence behaviour are compared with the genetic algorithm (GA), particle swarm optimization (PSO), cuckoo search algorithm (CSA), HSA and hybrid GA-nonlinear programming (GA-NLP) methods.
- performs a statistical analysis using descriptive and nonparametric tests to demonstrate the more excellent value of HSA-BB.

2. Problem Formulation of Optimum Relay Coordination

In the optimum coordination of relays, the foremost objective is to obtain relay settings that minimize the total operating time of relays under the coordination and boundary constraints. The objective function and the constraints formulation for optimum relay coordination are shown in the following sub-sections.

2.1. Objective Function (OF)

The OF, which needs to be minimized, is the sum of the operation times of relays when they act as primary relays [6].

$$OF = \sum_{i=1}^{k} TOP_i \tag{1}$$

where TOP_i indicates the time of the primary relay R_i, and k shows the number of primary relays.

2.2. Constraints

The desired constraints in the relay coordination problem should be satisfied while minimizing the OF. These constraints are formulated as follows.

2.2.1. Coordination Time Interval (CTI)

The time interval between the operating time of primary and backup (P/B) protection is essential for preserving selectivity. Its time interval is known as CTI, and it may be stated as:

$$t_b - t_p \geq CTI \tag{2}$$

where t_b and t_p are the operation of times in the order of backup and primary relays.

2.2.2. Bounds on Relay Settings

The DOCR has only two settings of the current pickup setting (I_{pi}) and time multiplier setting (TMS), whereas VROCR has an additional third setting of voltage pickup setting (V_{pi}).

The bounds on TMS of the relay may be defined as:

$$TMS^{\min} \leq TMS \leq TMS^{\max} \tag{3}$$

TMS range can be represented as a continuous value from 0.1 to 1.1 for DOCRs [5] and 0.05 to 1.1 for VROCRs [36].

The boundaries of I_{pi} of a relay can be presented as:

$$I_{pi}^{\min} \leq I_p \leq I_{pi}^{\max} \tag{4}$$

To ensure the security and reliability of protection schemes [6,7], I_{pi} is determined based on two parameters, the maximum full-load current and lowest fault current.

The boundaries of V_{pi} of the relay may be defined as:

$$V_{pi}^{\min} \leq V_p \leq V_{pi}^{\max} \tag{5}$$

The fault in the power network is attended by a related voltage dip, while the overload causes an only modest drop in voltage. Therefore, a voltage and current measurement-based fault detection relay—such as VROCR—can discriminate between overload and fault. VROCR becomes increasingly responsive to overcurrent as the voltage of the systems drops [37]. The V_{pi} range can be taken as a continuous value from 0% to 85% of the system nominal voltage.

2.2.3. Bounds on Time of Operation (TOP) of Relay

A certain minimum amount of operating time is needed for a relay. It should not take a long operating time. This constraint is defined as:

$$TOP^{\min} \leq TOP \leq TOP^{\max} \tag{6}$$

where TOP^{min} and TOP^{max} are the minimum and maximum operating times of the relay.

2.2.4. Characteristic of Relay

The inverse definite minimum time (IDMT) characteristic for DOCRs is widely used in the protection system [5–11]. It is defined as follows.

$$TOP = \left(\frac{0.14}{\left(\frac{I_f}{I_{pi}} \right)^{0.02} - 1} \right) TMS \tag{7}$$

where I_f is the fault current.

Based on the IEC 60255-3 standard, a VROCR characteristic is expressed as [36]:

$$TOP = \left(\frac{0.14}{\left(\frac{I}{I_{pi}} \times \frac{V_{pi}}{V} \right)^{0.02} - 1} \right) TMS \tag{8}$$

where V and I are the measured values of voltage and current by VROCR. I_{pi} and V_{pi} are the pickup settings of the current and voltage of VROCR, respectively.

3. Hybrid HSA-BB Method

The proposed hybrid HSA-BB approach is illustrated in this section. In the following sub-sections, a brief introduction of the HSA and BB is shown before explaining the hybridization of HSA-BB.

3.1. Harmony Search Algorithm

The HSA is a successful metaheuristic algorithm introduced by Geem et al. [38]. It is stimulated by the ideologies of the musicians' improvisation process for finding the best harmony. The flowchart for HSA is represented in Figure 1.

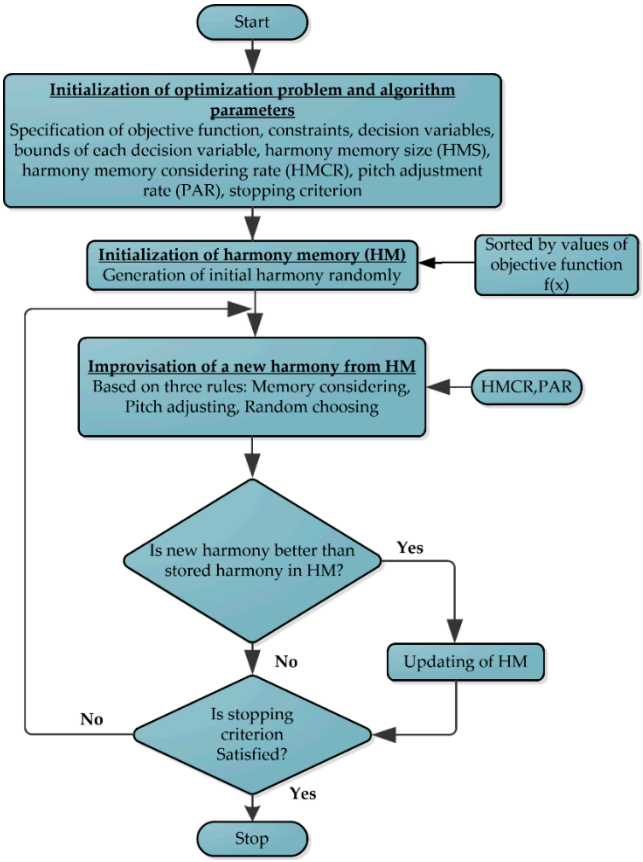

Figure 1. Flow diagram of the Harmony Search Algorithm (HSA).

The HSA can be executed in the following stages [8,38–41].

Step 1: Initialize the optimization problem and parameters of the algorithm:

For the HSA application, the OF with constraints and decision variables should be initialized as:

$$\begin{array}{lll} \textit{Minimize} & f(\vec{x}) & \\ \text{Subject to} & g_j(\vec{x}) \geq 0 & (j = 1, 2, \ldots, M), \\ & h_l(\vec{x}) = 0 & (l = 1, 2, \ldots, P), \\ & x_{i,L} \leq x_i \leq x_{i,U} & (i = 1, 2, \ldots, N) \end{array} \tag{9}$$

where $f(\vec{x})$ is the objective function, P and M represent the numbers of constraints, P (equality), and M (inequality). x_i shows the decision variables set, and N is the number of variables. The upper and lower boundaries for decision variables are represented in the order of $x_{i,U}$, and $x_{i,L}$. In this step, the algorithm parameters (i.e., harmony memory size (HMS), harmony memory consideration rate (HMCR), pitch adjustment rate (PAR)), and a maximum number of iterations are also provided.

All solution vectors are stored in the harmony memory (HM). Solution vectors are improvised using HMCR and PAR, as demonstrated in step 3.

Step 2: Initialize the HM:

In this step, the randomly generated solution vectors (x^1, ... , x^{HMS}) are stored in the HM, according to HMS. It is defined by the following equation.

$$HM = \begin{pmatrix} x_1^1 & \cdots & x_N^1 \\ \vdots & \ddots & \vdots \\ x_1^{HMS} & \cdots & x_N^{HMS} \end{pmatrix} \tag{10}$$

It is possible that infeasible solutions with violated constraints arise. When this occurs, the algorithm forces the search towards a feasible solution area using the static penalty function.

Step 3: Generate a new harmony by improvising the stored harmony in the HM:

A new vector of harmony $\vec{x} = \left(x_1', \ x_2', \ldots, x_N'\right)$ is formed according to the HMCR, PAR, and a random selection, which is called improvisation. According to the HMCR, ith variable of $x_i^1 = \left(x_L^1 - x_{HMS}^1\right)$ can be improvised using Equation (11). HMCR is the probability of selecting a value from the stored value in the HM, whereas (1-HMCR) is the probability of randomly generating a new value. The range of HMCR is defined between 0 and 1.

$$x_i' \leftarrow \begin{cases} x_i' \in \left\{x_i^1, x_i^2, \ldots, x_i^{HMS}\right\} & \text{with probability HMCR} \\ x_i' \in X_i & \text{with probability (1-HMCR)} \end{cases} \tag{11}$$

If $x_i^{'}$ is selected from the HM, it is further tuned using PAR. PAR represents the probability of a component from the HM mutating, while (1-PAR) shows the probability of no mutation. It is expressed using the following equation.

$$x_i' \leftarrow \begin{cases} x_i' \pm rand[0,1] \times b_w & \text{with probability PAR} \\ x_i' & \text{with probability (1-PAR)} \end{cases} \tag{12}$$

where rand [0, 1] represents the randomly generated value in the range of 0 and 1. b_w is the bandwidth of arbitrary distance for the design variable.

Step 4: Update the HM:

If, according to the OF value, a newly generated vector is better than the worst one that existed in the HM, the worst should be replaced by a new one.

Step 5: Check the criterion for stopping the algorithm:

Step 3 and step 4 are repeated until a stopping criterion (e.g., maximum numbers of iteration) has been met.

3.2. Bollinger Bands Approach

The Bollinger Bands method is widely used to forecast the upcoming prices of the stocks. It was developed by J. Bollinger [42]. Based on historical data, it computes the mean and standard deviation of the prices for estimating the interval. The BB for each decision variable can be premeditated using the following terms.

The mean is considered as a middle band and can be calculated for decision variable x_i as:

$$\overline{x}_i = \frac{\sum_{c=1}^{n} x_i^c}{n} \tag{13}$$

where n is the number of available samples of each variable.

The standard deviation for decision variable xi is calculated as:

$$\sigma_i = \sqrt{\frac{\sum_{c=1}^{n} \left(x_i^c - \overline{x}_i\right)^2}{n}} \tag{14}$$

For decision variable x_i, the upper and lower bands are calculated using the following expression.

$$UB_i = \overline{x}_i + (a \cdot \sigma_i) \tag{15}$$

$$LB_i = \overline{x}_i - (a \cdot \sigma_i) \tag{16}$$

where UB_i and LB_i are the upper and lower bands. a is the constant value and selected in the range of 1 to 2.

Further, the x_i is updated by the following equation.

$$x_i' = LB_i + (UB_i - LB_i) \times r \tag{17}$$

where $x_i^{'}$ is a newly generated value for variable x, and r is a randomly generated value between 0 and 1.

3.3. Hybrid HSA-BB Method

Exploration and exploitation are important parameters for metaheuristic methods. Exploration parameters ensure that algorithms will not be biased in local optima. Exploitation parameters exploit previous solutions for reducing the randomization, which ultimately helps the algorithm in faster convergence. Very strong exploitation can cause the slowing down of the exploration, which ultimately leads to premature convergence and an insignificant solution. To deal with this issue and to develop a more efficient algorithm, different search strategies are hybridized in the literature [6,7,9,39,43]. Similarly, the HSA is useful for exploring to find nearby global regions, but it has a problem of searching the local optima [39]. On the other hand, BB has good exploiting history, since it utilizes all previous components while generating new ones. Therefore, in this study, the HSA is hybridized with BB to enhance the performance of HSA in terms of a local search, accuracy of results, and convergence. Also, BB is modified to help the HSA in exploration during the initial generation and in exploitation during the final generation. The HSA and BB are hybridized as follows.

1. Adaptive Bollinger band: The value of a when calculating the upper and lower bands in BB is illustrated by Equations (15) and (16), and fixed between 1 and 2. However, a higher value of a can cause a larger gap between the upper and lower bands, and a lower value of a makes this gap smaller. From Equation (17), it is clear that during the early generations, smaller gaps will provide smaller values when updating the current value of the component (x_i), which ultimately affects exploration. However, any algorithm should be good at exploring during early generations, so that it may not be trapped in local optima. On the other hand, during final generations, a larger gap will provide a larger value while updating the current component (x_i), which ultimately affects the exploitation. As discussed earlier, weak exploitation slows down the convergence performance of algorithms. To deal with this problem, the parameter a in Equations (15) and (16) is modified such a way that it dynamically changes with each generation. It is shown by the following equation.

$$a = \frac{(2 \cdot NI - gn)}{NI} \tag{18}$$

where NI represents the maximum number of iterations, whereas gn shows the generation number.

2. Using Equation (12), HSA performs a local search. This equation is modified using Equation (17) of BB. Initially, the HSA completes the course search by using randomization and HMCR and fills the HM. Using the solution vectors stored in the HM, BB calculates the mean and standard deviation as

well as the lower and upper bands for each decision variable as given by Equations (13)–(16). It is also noted that the number of samples n is equal to the HMS. Suppose that HMS is considered as 30, then the available number of sample values of each decision variable is 30. Afterward, a new value for each decision variable is computed by Equation (17) of BB in the local search step of HSA (Equation (12) in step 3). This is illustrated as follows.

$$x_i' \leftarrow \begin{cases} x_i' = LB_i + (UB_i - LB_i) \times r & \text{with probability PAR} \\ x_i' & \text{with probability (1-PAR)} \end{cases} \quad (19)$$

If the new solution vector of decision variables is better than the worst one stored in the HM, then the worst vector is replaced with new one. The remaining steps of the proposed hybrid approach are the same as the HSA, which is already discussed in Section 3.1.

4. Simulation Results and Discussion

The performance of a proposed hybrid HSA-BB approach for the optimal coordination of DOCRs-DOCRs and DOCRs-VROCRs is verified on SPVGs connected-three different power networks. The first test case has 14 DOCRs and 1 VROCR, the second has 24 DOCRs and 4 VROCRs, and the third has 78 DOCRs and 3 VROCRs. The SPVG is designed based on the data given in [1,35,44–46]. ETAP software is used for modeling and fault calculation of SPVG-connected networks. Ranges of TMS are considered in all cases, from 0.1 to 1.1 for DOCRs and 0.05 to 1.1 for VROCRs, respectively. The minimum time of operation of each relay and CTI are assumed in order of 0.2 and 0.3 s for test cases 1 and 2. Both are considered to be 0.2 s in test case 3. Simulation outcomes are compared with GA, PSO, CSA, HSA, and GA-NLP for demonstrating the effectiveness of the HSA-BB. The comparative study is conducted in terms of convergence behavior and statistical analysis for an IEEE 30-bus system. The parameter values for all algorithms are given in Table 1.

Table 1. Parameter values of all algorithms for each test system.

Method	Parameters	8-Bus System	9-Bus System	IEEE 30-Bus System
GA	Population size (P_s)	150	200	300
	Crossover rate (CR)	0.95	0.95	0.95
	Mutation rate (MR)	0.01	0.01	0.01
PSO	Numbers of particles (N)	30	50	100
	Acceleration coefficients ($C1$, $C2$)	(2.1, 2.0)	(2.1, 2.0)	(2.1, 2.0)
	Min. and max. inertia weights (w_{min}, w_{max})	(0.2, 1.0)	(0.2, 1.0)	(0.2, 1.0)
	Min. and max. velocity (v_{min}, v_{max})	(−0.45, 0.45)	(−0.45, 0.45)	(−0.45, 0.45)
CSA	Numbers of nets (n)	20	25	35
	Discovery rate (P_a)	0.25	0.25	0.25
HSA	Harmony memory size (HMS)	30	30	40
	Harmony memory consideration rate (HMCR)	0.9	0.9	0.9
	Pitch adjustment rate (PAR)	0.5	0.5	0.5

4.1. Case 1: 8-Bus Network

The proposed hybrid approach is implemented on a 40 MW SPVG-connected eight-bus network with a voltage rating of 150 kV. A minimum rating of 40 MW is required for SPVG if it is connected to the high voltage grid of 132 kV or above [1]. Accordingly, the 40 MW SPVG is designed, and it supplies 150 A current to the eight-bus network through bus 5, as shown in Figure 2. The data for the eight-bus network were provided in [47].

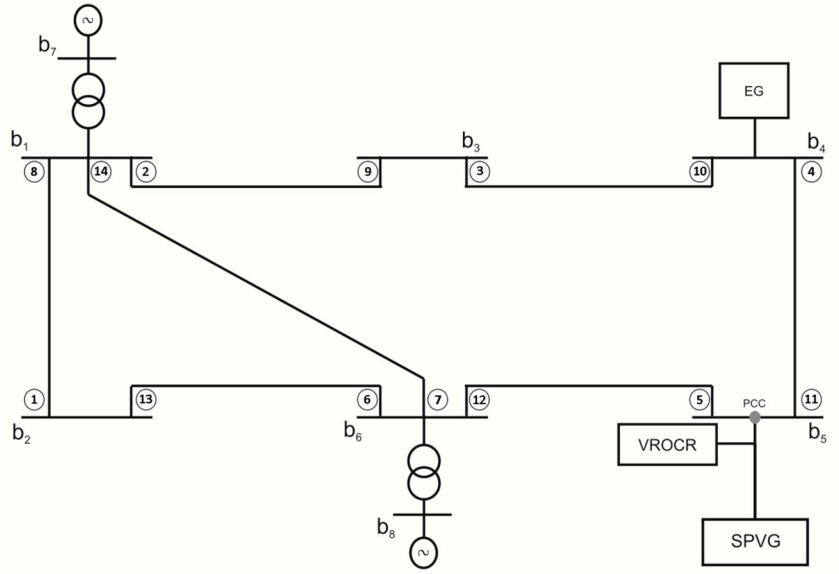

Figure 2. Diagram of SPVG-connected 8-bus system.

Table 2 lists the results of the current magnitude for close-in 3-Φ fault current and P/B DOCRs pairs. Table 3 contains the voltage and current sensed by VROCR for a close-in fault to each DOCR. It is learned from Table 3 that VROCR senses the maximum fault current (1.45 times the rated current supplied by SPVG) for the close-in fault to relays 5 and 11. The voltage drop (0% of system nominal voltage) is also maximum in this case. Similarly, the minimum fault current (1.15 times the rated current supplied by SPVG) and voltage drop (20.42 % of system nominal voltage) are sensed by VROCR for the close-in fault to relays 1 and 13. As shown in Figure 3, the VROCR trips for the current above 110% of the full load current supplied by SPVG, and voltage drops below 85% of the system nominal voltage. The voltage sensed by VROCR is 0 kV for the close-in fault to relays 5 and 11. The characteristic of VROCR presented by Equation (8) becomes undefined. Hence, the maximum value of 20 is assumed for $\left(\frac{I}{I_{pi}} \times \frac{V_{pi}}{V}\right)$ in Equation (8) for the close-in fault to relay 5 and 11 in this case.

Table 2. Fault current for primary and backup (P/B) directional overcurrent relays (DOCRs) pairs of 8-bus network.

Primary Relay (PR)	Fault Current (A)	Backup Relay (BR)	Fault Current (A)	Primary Relay (PR)	Fault Current (A)	Backup Relay (BR)	Fault Current (A)
1	3382	6	3382	8	6278	7	2068
2	6098	1	1000	8	6278	9	1180
2	6098	7	2068	9	2635	10	2635
3	3560	2	3560	10	4060	11	2520
4	3790	3	2250	11	3917	12	3700
5	2617	4	2400	12	5899	13	989
6	6293	5	1383	12	5899	14	1880
6	6293	14	1880	13	3075	8	3075
7	5402	5	1383	14	5220	1	1000
7	5402	13	989	14	5220	9	1180

Table 3. Measured quantities by VROCR for the close-in fault to each DOCR of 8-bus network.

Close-in Fault to DOCRs	VROCR as Backup			
Relay No.	**Voltage Reduction (kV)**	**Voltage Reduction in (%) of System Voltage**	**Fault Current Supplied by SPVG (A)**	**Fault Current in (%) of Rated Current Supplied by SPVG**
1	30.63	20.42	173	115.33
2	18.29	12.19	191	127.33
3	28.80	19.20	175	116.67
4	18.68	12.45	190	126.67
5	0.00	0.00	217	144.67
6	9.76	06.51	203	135.33
7	9.76	06.51	203	135.33
8	18.29	12.19	191	127.33
9	28.80	19.20	175	116.67
10	18.68	12.45	190	126.67
11	0.00	0.00	217	144.67
12	9.76	06.51	203	135.33
13	30.63	20.42	173	115.33
14	18.29	12.19	191	127.33

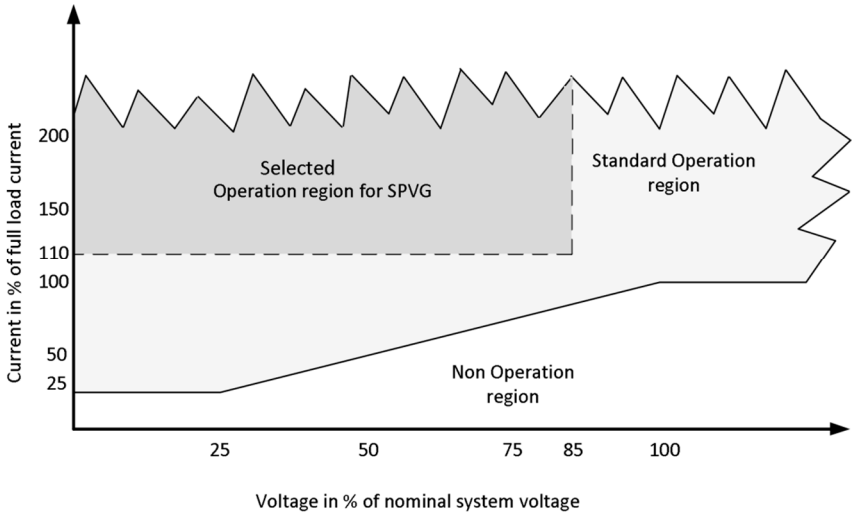

Figure 3. Voltage-restrained overcurrent relay (VROCR) operating characteristics based on pickup settings of current and voltage for SPVG protection.

By implementing all methods, the obtained results of relay settings, TOP of primary relays, and OF value formed by using Equation (1) are displayed in Table 4. HSA-BB provides the best minimized OF (9.636 s) compared to hybrid GA-NLP (9.795 s), HSA (12.325 s), CSA (12.533 s), PSO (14.417 s) and GA (16.916 s). The CTI between P/B DOCRs-DOCRs and DOCRs-VROCR is tabulated in Table 5. As seen from this result, the CTI is maintained at a minimum level (0.3 s) for almost all P/B DOCRs-DOCRs pairs in HSA-BB as compared to other stated methods. The CTI of P/B DOCRs-VROCR pairs is also minimal in HSA-BB as compared to other methods. As the HSA-BB gives better results than other employed methods, further analysis of VROCR operation is discussed only for the results obtained by HSA-BB.

Table 4. Results of 8-bus network.

Relay No.	GA				PSO				CSA				HSA				GA-NLP				HSA-BB			
	Ipi (A)	**Vpi (kV)**	**TMS**	**TOP (s)**	**Ipi (A)**	**Vpi (kV)**	**TMS**	**TOP (s)**	**Ipi (A)**	**Vpi (kV)**	**TMS**	**TOP (s)**	**Ipi (A)**	**Vpi (kV)**	**TMS**	**TOP (s)**	**Ipi (A)**	**Vpi (kV)**	**TMS**	**TOP (s)**	**Ipi (A)**	**Vpi (kV)**	**TMS**	**TOP (s)**
1	300.0	–	0.289	0.816	592.6	–	0.113	0.445	385.4	–	0.178	0.561	459.1	–	0.145	0.499	508.8	–	0.105	0.380	524.5	–	0.100	0.369
2	302.0	–	0.551	1.245	405.8	–	0.470	1.182	439.4	–	0.383	0.993	489.5	–	0.368	0.994	598.3	–	0.264	0.778	600.0	–	0.264	0.778
3	202.5	–	0.516	1.224	288.4	–	0.429	1.164	233.5	–	0.381	0.953	201.5	–	0.409	0.969	449.8	–	0.217	0.719	450.0	–	0.217	0.718
4	517.0	–	0.337	1.162	308.5	–	0.365	0.993	462.5	–	0.258	0.841	341.8	–	0.297	0.844	599.7	–	0.168	0.628	600.0	–	0.168	0.627
5	369.6	–	0.346	1.212	417.5	–	0.245	0.919	407.2	–	0.211	0.780	474.8	–	0.183	0.736	599.9	–	0.115	0.538	600.0	–	0.115	0.538
6	300.0	–	0.426	0.949	312.6	–	0.279	0.632	345.2	–	0.287	0.673	306.5	–	0.287	0.645	473.7	–	0.195	0.514	354.4	–	0.220	0.521
7	200.0	–	0.669	1.373	264.7	–	0.458	1.031	228.2	–	0.417	0.893	252.9	–	0.397	0.880	449.9	–	0.239	0.656	450.0	–	0.238	0.655
8	300.0	–	0.453	1.011	374.9	–	0.255	0.616	328.0	–	0.297	0.683	301.5	–	0.287	0.642	468.9	–	0.192	0.505	359.0	–	0.216	0.513
9	200.5	–	0.339	0.897	373.4	–	0.240	0.844	309.5	–	0.216	0.691	295.2	–	0.215	0.673	449.9	–	0.133	0.516	450.0	–	0.129	0.504
10	300.8	–	0.380	0.995	314.9	–	0.382	1.019	349.2	–	0.292	0.814	412.8	–	0.263	0.788	599.6	–	0.175	0.629	600.0	–	0.172	0.619
11	300.8	–	0.402	1.068	384.4	–	0.363	1.068	591.6	–	0.234	0.850	353.3	–	0.312	0.887	485.2	–	0.222	0.729	600.0	–	0.191	0.700
12	301.5	–	0.503	1.149	339.1	–	0.483	1.150	498.1	–	0.337	0.930	374.6	–	0.398	0.983	503.7	–	0.299	0.830	600.0	–	0.265	0.792
13	300.5	–	0.350	1.029	519.4	–	0.135	0.523	321.1	–	0.200	0.606	434.4	–	0.152	0.534	554.1	–	0.100	0.402	523.1	–	0.100	0.388
14	201.3	–	0.474	0.985	203.6	–	0.498	1.040	245.1	–	0.367	0.814	400.4	–	0.289	0.768	449.9	–	0.234	0.653	450.0	–	0.226	0.631
VR-OCR	166.5	127.5	0.794	1.800	166.5	127.5	0.790	1.791	166.5	127.5	0.640	1.451	166.5	127.5	0.653	1.481	166.5	127.5	0.582	1.319	166.5	127.5	0.566	1.283
OF (s)	16.916				14.417				12.533				12.325				9.795				9.636			

Table 5. Coordination time interval (CTI) values of P/B relay pairs for 8-bus system.

P/B Relay Pair	CTI (s)						P/B Relay Pair	CTI (s)					
	GA	PSO	CSA	HSA	GA-NLP	HSA-BB		GA	PSO	CSA	HSA	GA-NLP	HSA-BB
1-6	0.384	0.357	**0.300**	0.318	**0.300**	**0.300**	13-8	0.301	0.308	0.302	0.311	**0.300**	**0.300**
2-1	0.417	0.316	0.302	0.302	**0.300**	**0.300**	14-1	0.677	0.458	0.481	0.529	0.426	0.447
2-7	0.712	0.345	0.302	0.301	**0.300**	**0.300**	14-9	0.328	0.405	0.300	0.304	**0.300**	**0.300**
3-2	0.301	0.318	0.302	0.302	**0.300**	**0.300**	1-VROCR	2.924	3.277	2.453	2.578	2.359	**2.297**
4-3	0.302	0.438	0.310	0.314	**0.300**	**0.300**	2-VROCR	1.373	1.424	1.117	1.160	1.139	**1.088**
5-4	0.303	0.301	**0.300**	0.311	**0.300**	**0.300**	3-VROCR	2.336	2.378	1.916	1.960	1.889	**1.819**
6-5	0.860	0.786	0.521	0.538	0.442	**0.434**	4-VROCR	1.491	1.647	1.297	1.338	1.315	**1.264**
6-14	0.501	0.901	**0.562**	0.643	0.617	0.571	5-VROCR	0.589	0.872	**0.671**	0.745	0.780	0.745
7-5	0.436	0.387	0.301	0.303	**0.300**	**0.300**	6-VROCR	1.004	1.312	0.901	0.961	0.917	**0.871**
7-13	0.659	0.429	0.337	0.405	**0.546**	**0.437**	7-VROCR	0.580	0.913	**0.681**	0.727	0.775	0.737
8-7	0.946	0.911	0.611	0.653	0.573	**0.565**	8-VROCR	1.608	1.989	1.427	1.512	1.412	**1.353**
8-9	**0.303**	0.829	0.431	0.430	0.448	0.418	9-VROCR	2.664	2.698	2.178	2.256	2.092	**2.034**
9-10	0.301	0.388	0.301	0.303	**0.300**	**0.300**	10-VROCR	1.659	1.621	1.324	1.395	1.315	**1.272**
10-11	0.301	0.305	0.300	0.303	**0.300**	**0.300**	11-VROCR	0.732	0.723	0.601	0.595	0.590	**0.583**
11-12	**0.300**	0.312	0.301	0.303	**0.300**	**0.300**	12-VROCR	0.805	0.794	0.644	0.624	**0.600**	**0.600**
12-13	0.884	0.310	0.300	0.302	0.371	**0.300**	13-VROCR	2.711	3.199	2.409	2.543	2.338	**2.278**
12-14	0.302	0.383	0.305	0.305	**0.300**	**0.300**	14-VROCR	1.633	1.566	1.296	1.386	1.265	**1.236**

The bold digits represent the minimum CTI value.

For the close-in fault to relay 5 and 11, the CTI of relay pairs 5-VROCR and 11-VROCR is 0.745 and 0.583 s, respectively. For the close-in fault to relay 6 and 7, relay 5 operates as the first backup and VROCR as a second backup. The CTI of relay pairs 6-5 and 7-5 are 0.4340 and 0.3 s, respectively. Thus, VROCR should operate after a minimum CTI of 0.7340 s (0.4340 + 0.3) and 0.6 s (0.3 + 0.3) for the close-in fault to relays 6 and 7. As shown in Table 5, VROCR operates after 0.8711 and 0.7371 s for the close-in fault to relays 6 and 7, respectively. In the case of close-in fault to relay 10, relay 11 as the first backup operates after 0.3 s time interval. Therefore, VROCR as the second backup should trip after 0.6 s. However, VROCR operates over a long time of 1.2720 s because VROCR senses less voltage reduction and fault current for the close-in fault to relay 10 than a close-in fault to relay 6 and 7, as shown in Table 3. For the close-in fault to relay 1, 2, and 8, VROCR works as a third backup. The CTI of relay pair 1-VROCR (2.2964 s) is more extensive than relay pairs 2-VROCR (1.0884 s) and 8-VROCR (1.3533 s), since VROCR experiences minimum voltage reduction and fault current for the close-in fault to relay 1 as shown in Table 3. The CTI of relay pair 2-7 (0.3 s) is less than the CTI of relay pair 8-7 (0.5649 s). Thus, VROCR trips over a long time to the close-in fault to relay 8 than the close-in fault to relay 2. For the close-in fault to relay 9, VROCR also works as a third backup and operates over 2.0340 s. This is because it experiences a moderate voltage reduction and fault current compared to relays 1, 2, and 8. With the final results of CTI of DCORs-VROCR, it can be deduced that the operation of VROCR depends on sensing the voltage reduction and fault current supplied by the SPVG as well as its action as backup protection.

4.2. Case 2: 9-Bus Network

In this case, four SPVG-connected systems with nine buses (b_1 to b_9) are considered (Figure 4). An SPVG of 8–10 MW is required for connecting to a 30–34.5 kV grid [1]. Therefore, each SPVG is designed with ratings of 8 MW and 33 kV. These are connected as $SPVG_1$ at b_7, $SPVG_2$ at b_5, $SPVG_3$ at b_9, and $SPVG_4$ at b_3. Each SPVG supplies the current of 138 A to the network. The external grid (EG) with 400-MVA short circuit capacity is connected to b_1. The impedance of each line segment is (0.0057 + j0.071) Ω/km. The current magnitude for close-in 3-Φ fault sensed by P/B pairs of DOCRs is provided in Table 6.

Table 7 shows the voltage and current sensed by VROCRs for the close-in fault to each DOCR. It can be seen that maximum fault current and voltage drop are sensed by VROCR1 for the close-in fault to relay 1, 16 and 18, by VROCR2 for the close-in fault to relay 12, 13 and 22, by VROCR3 for the close-in fault to relay 4 and 5, and by VROCR4 for the close-in fault to relay 8 and 9. Similarly, the minimum fault current and voltage drop are experienced by VROCR1 and VROCR3 for the close-in fault to relay 10 and 11, and VROCR2 and VROCR4 for the close-in fault to relay 2 and 3, respectively.

Table 8 shows the use of all the approaches, and the results of relay settings, the TOP of primary relays and the OF value. It is seen from Table 8 that the OF value acquired by using HSA-BB is less as compared to GA, PSO, CSA, HSA, and GA-NLP. The CTI value derived for P/B DOCRs-DOCRs and DOCRs-VROCRs pairs for the close-in fault to each DOCR is presented in Tables 9 and 10, respectively. It is seen in Tables 9 and 10 that all the coordination constraints have been satisfied when determining the results of these methods. Also, the larger value of CTI shows the larger operating time of backup relays, which is not desirable for a protection system. In Table 9, the obtained value of CTI for P/B DOCRs-DOCRs pairs is almost maintained to the minimum prescribed level in the results of HSA-BB. Also, the fast operating time of VROCR may raise unnecessary isolation of SPVG if it is used as a backup of DOCRs, thus putting grid network stability at risk [1]. As shown in Table 10, the purpose of the larger CTI value for DOCRs-VROCRs pairs (i.e., 10-VROCR1 and 11-VROCR1, 2-VROCR2 and 3-VROCR2, 10-VROCR3 and 11-VROCR3, 2-VROCR4 and 3-VROCR4) is to ride through disturbances for avoiding the undesirable removal of SPVG. Therefore, a less sensitive setting is preferred for the VROCR when it needs to operate as a backup of DOCRs, especially for the far fault to the VROCR.

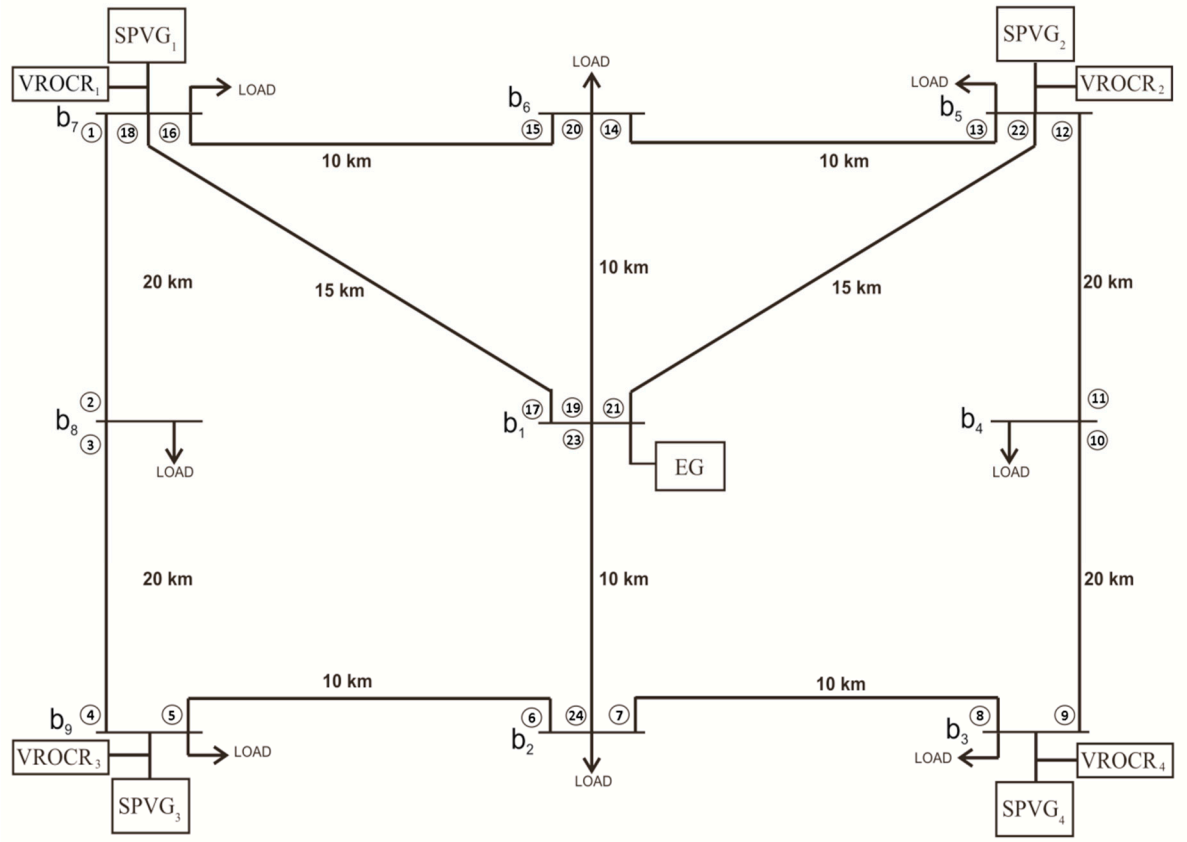

Figure 4. Diagram of a four SPVG-connected 9-bus system.

Table 6. Fault current for P/B DOCR pairs of 9-bus system.

PR	Fault Current (A)	BR	Fault Current (A)	PR	Fault Current (A)	BR	Fault Current (A)
1	5817	15	2636	16	3940	2	759
1	5817	17	2980	16	3940	17	2980
2	2338	4	2338	17	8091	20	168
3	3145	1	3145	17	8091	22	122
4	4206	6	4005	17	8091	24	301
5	1731	3	1530	18	3596	2	759
6	5666	8	976	18	3596	15	2636
6	5666	23	4690	19	8091	18	122
7	5666	5	976	19	8091	22	122
7	5666	23	4690	19	8091	24	301
8	1731	10	1530	20	3508	13	1754
9	4206	7	4206	20	3508	16	1754
10	3145	12	3145	21	8091	18	122
11	2338	9	2338	21	8091	20	168
12	5811	14	2630	21	8091	24	301
12	5811	21	2980	22	3596	11	759
13	3940	11	759	22	3596	14	2636
13	3940	21	2980	23	7912	18	122
14	5244	16	1754	23	7912	20	122
14	5244	19	3490	23	7912	22	168
15	5244	13	1754	24	1952	5	976
15	5244	19	3490	24	1952	8	976

Table 7. Measured quantities by VROCRs for the close-in fault to each DOCR of the 9-bus network.

Close-in Fault to DOCRs	VROCR1		VROCR2		VROCR3		VROCR4	
Relay No.	Voltage Reduction (kV)	Fault Current Supplied by $SPVG_1$(A)	Voltage Reduction (kV)	Fault Current Supplied by $SPVG_2$(A)	Voltage Reduction (kV)	Fault Current Supplied by $SPVG_3$(A)	Voltage Reduction (kV)	Fault Current Supplied by $SPVG_4$(A)
1	0.00	201	4.26	175	3.76	179	4.61	173
2	7.53	155	9.62	148	5.50	168	8.52	149
3	7.53	155	9.62	148	5.50	168	8.52	149
4	7.58	155	8.32	151	0.00	201	5.67	167
5	7.58	155	8.32	151	0.00	201	5.67	167
6	4.90	171	4.90	171	1.05	195	1.05	195
7	4.90	171	4.90	171	1.05	195	1.05	195
8	8.32	152	7.58	155	5.67	167	0.00	201
9	8.32	152	7.58	155	5.67	167	0.00	201
10	9.62	148	7.53	155	8.52	149	5.50	168
11	9.62	148	7.53	155	8.52	149	5.50	168
12	4.26	175	0.00	201	4.61	173	3.76	179
13	4.26	175	0.00	201	4.61	173	3.76	179
14	1.99	189	1.99	189	3.45	180	3.45	180
15	1.99	189	1.99	189	3.45	180	3.45	180
16	0.00	201	4.26	175	3.76	179	4.61	173
17	0.31	201	0.31	201	0.56	201	0.56	201
18	0.00	201	4.26	175	3.76	179	4.61	173
19	0.31	201	0.31	201	0.56	201	0.56	201
20	1.99	189	1.99	189	3.45	180	3.45	180
21	0.31	201	0.31	201	0.56	201	0.56	201
22	4.26	175	0.00	201	4.61	173	3.76	179
23	0.31	201	0.31	201	0.56	201	0.56	201
24	4.90	171	4.90	171	1.05	195	1.05	195

4.3. Case 3: IEEE 30-Bus Network

To confirm the success of the proposed hybrid approach, its performance needs to be demonstrated using a larger and more complex system. For this task, the IEEE 30-bus network is selected, as shown in Figure 5. It can be considered as a meshed sub-transmission and distribution system [10]. This complex power network has 30 buses (132 kV and 33 kV buses), 37 lines, 78 DOCRs and 3 VROCRs. In addition, three SPVGs with the rating of 8 MW are connected to the distribution network (33 kV) as $SPVG_1$ at b_{19}, $SPVG_2$ at b_{22} and $SPVG_3$ at b_{23}. As it includes VROCRs, the total number of constraints increased to 666 as compared to 426 when considering only DOCRs in the test system. Thus, optimization methods have to consider highly constrained optimization problems in this test case.

Table 8. Results of 9-bus network.

Relay No.	GA				PSO				CSA				HSA				GA-NLP				HSA-BB			
	Ipi (A)	Vpi (kV)	TMS	TOP (s)	Ipi (A)	Vpi (kV)	TMS	TOP (s)	Ipi (A)	Vpi (kV)	TMS	TOP (s)	Ipi (A)	Vpi (kV)	TMS	TOP (s)	Ipi (A)	Vpi (kV)	TMS	TOP (s)	Ipi (A)	Vpi (kV)	TMS	TOP (s)
1	178.3	—	0.449	0.870	404.3	—	0.359	0.918	328.7	—	0.400	0.837	227.6	—	0.400	0.837	572.3	—	0.241	0.711	599.9	—	0.203	0.612
2	256.3	—	0.175	0.540	250.7	—	0.177	0.543	423.8	—	0.150	0.504	302.0	—	0.150	0.503	422.3	—	0.100	0.402	360.5	—	0.100	0.367
3	128.1	—	0.360	0.763	104.2	—	0.454	0.901	355.8	—	0.246	0.740	323.6	—	0.246	0.739	373.2	—	0.209	0.672	400.0	—	0.164	0.545
4	99.1	—	0.393	0.707	286.1	—	0.259	0.656	312.2	—	0.227	0.613	336.1	—	0.227	0.613	344.2	—	0.196	0.535	399.9	—	0.171	0.498
5	381.7	—	0.152	0.692	219.4	—	0.256	0.850	277.6	—	0.269	0.790	169.1	—	0.269	0.790	273.5	—	0.193	0.720	485.2	—	0.100	0.543
6	131.0	—	0.510	0.912	118.5	—	0.500	0.871	228.5	—	0.300	0.789	424.4	—	0.300	0.789	293.3	—	0.321	0.737	409.0	—	0.266	0.690
7	166.5	—	0.429	0.821	407.2	—	0.341	0.883	441.4	—	0.276	0.754	466.7	—	0.276	0.754	291.3	—	0.327	0.749	363.2	—	0.280	0.695
8	200.1	—	0.279	0.885	337.9	—	0.179	0.756	208.7	—	0.138	0.656	405.3	—	0.138	0.656	252.5	—	0.203	0.725	483.7	—	0.100	0.542
9	173.7	—	0.289	0.614	270.5	—	0.290	0.720	66.7	—	0.283	0.578	153.8	—	0.283	0.578	388.3	—	0.188	0.539	390.0	—	0.173	0.498
10	400.0	—	0.230	0.766	296.4	—	0.252	0.729	359.0	—	0.251	0.679	252.7	—	0.251	0.679	380.9	—	0.207	0.672	400.0	—	0.164	0.544
11	384.4	—	0.120	0.457	194.0	—	0.227	0.622	241.6	—	0.100	0.404	425.2	—	0.100	0.404	371.9	—	0.112	0.418	356.1	—	0.100	0.365
12	189.5	—	0.321	0.633	178.7	—	0.368	0.714	160.5	—	0.362	0.690	167.8	—	0.362	0.690	152.7	—	0.303	0.562	152.0	—	0.254	0.470
13	161.3	—	0.436	0.925	339.9	—	0.304	0.847	250.4	—	0.392	0.863	181.5	—	0.392	0.863	171.7	—	0.365	0.789	400.0	—	0.207	0.618
14	183.3	—	0.436	0.880	182.5	—	0.447	0.901	158.6	—	0.314	0.801	362.4	—	0.314	0.801	242.5	—	0.369	0.816	400.0	—	0.259	0.688
15	122.4	—	0.529	0.949	152.0	—	0.511	0.975	133.3	—	0.404	0.880	233.5	—	0.403	0.880	320.7	—	0.313	0.762	399.9	—	0.250	0.664
16	278.7	—	0.316	0.813	325.2	—	0.295	0.806	234.7	—	0.402	0.826	145.6	—	0.402	0.826	94.5	—	0.480	0.868	400.0	—	0.212	0.633
17	602.2	—	0.283	0.743	704.7	—	0.255	0.713	526.1	—	0.296	0.723	497.3	—	0.296	0.723	496.5	—	0.306	0.746	567.7	—	0.225	0.577
18	81.3	—	0.113	0.200	118.5	—	0.101	0.200	107.4	—	0.109	0.200	90.4	—	0.109	0.200	92.7	—	0.109	0.202	92.7	—	0.108	0.200
19	653.1	—	0.362	0.982	703.3	—	0.297	0.829	680.1	—	0.286	0.778	656.9	—	0.286	0.778	720.0	—	0.257	0.726	775.1	—	0.216	0.628
20	112.1	—	0.102	0.200	133.8	—	0.100	0.207	134.4	—	0.110	0.217	112.9	—	0.110	0.217	120.1	—	0.100	0.201	118.2	—	0.100	0.200
21	471.6	—	0.350	0.838	781.2	—	0.223	0.651	628.2	—	0.308	0.744	484.3	—	0.308	0.744	493.8	—	0.285	0.694	562.9	—	0.229	0.586
22	81.3	—	0.222	0.395	92.4	—	0.109	0.200	100.1	—	0.109	0.200	91.4	—	0.109	0.200	96.5	—	0.107	0.200	91.7	—	0.109	0.200
23	778.4	—	0.325	0.958	788.1	—	0.307	0.911	768.7	—	0.291	0.854	768.1	—	0.291	0.854	769.7	—	0.279	0.817	800.0	—	0.256	0.764
24	200.7	—	0.206	0.618	205.1	—	0.100	0.304	212.9	—	0.100	0.309	212.5	—	0.100	0.309	213.6	—	0.100	0.310	200.8	—	0.100	0.301
VROCR1	151.8	28.05	1.082	1.205	151.8	28.05	1.094	1.219	151.8	28.05	1.025	1.142	151.8	28.05	1.025	1.142	151.8	28.05	1.072	1.195	151.8	28.05	0.838	0.933
VROCR2	151.8	28.05	1.100	1.225	151.8	28.05	1.031	1.149	151.8	28.05	1.066	1.188	151.8	28.05	1.066	1.187	151.8	28.05	0.989	1.102	151.8	28.05	0.824	0.918
VROCR3	151.8	28.05	1.100	1.225	151.8	28.05	1.010	1.125	151.8	28.05	0.883	0.983	151.8	28.05	0.883	0.983	151.8	28.05	0.938	1.045	151.8	28.05	0.756	0.842
VROCR4	151.8	28.05	0.947	1.055	151.8	28.05	1.045	1.164	151.8	28.05	0.983	1.095	151.8	28.05	0.983	1.095	151.8	28.05	0.922	1.027	151.8	28.05	0.757	0.843
OF (s)	21.874				21.364				20.263				19.835				18.943				15.964			

Table 9. CTI of P/B DOCRs-DOCRs pairs of 9-bus network.

P/B Relay Pair	CTI (s)						P/B Relay Pair	CTI (s)					
	GA	PSO	CSA	HSA	GA-NLP	HSA-BB		GA	PSO	CSA	HSA	GA-NLP	HSA-BB
1-15	**0.300**	**0.300**	**0.300**	**0.300**	0.307	**0.300**	16-2	**0.300**	0.302	0.375	0.305	0.319	**0.300**
1-17	0.349	0.301	0.306	0.300	0.463	0.321	16-17	0.406	0.413	0.301	0.311	0.306	**0.300**
2-4	0.303	0.301	**0.300**	**0.300**	0.301	**0.300**	17-20	**1.012**	2.355	2.426	1.212	1.331	1.412
3-1	**0.300**	**0.300**	**0.300**	**0.300**	0.302	**0.300**	17-22	3.074	**2.018**	3.051	1.906	2.459	2.079
4-6	0.301	0.304	**0.300**	**0.300**	0.303	**0.300**	17-24	2.791	**1.105**	1.311	1.281	1.288	1.146
5-3	**0.300**	**0.300**	**0.300**	0.301	0.302	**0.300**	18-2	0.913	0.907	0.994	0.930	0.986	**0.733**
6-8	**0.300**	0.301	**0.300**	0.301	0.301	**0.300**	18-15	0.970	1.018	0.915	0.937	0.816	**0.712**
6-23	0.332	0.313	0.450	0.318	0.323	**0.305**	19-18	**0.953**	23.238	4.909	1.772	2.053	2.129
7-5	**0.300**	**0.300**	**0.300**	**0.300**	0.301	**0.300**	19-22	2.835	1.902	2.969	**1.850**	2.480	2.027
7-23	0.423	0.301	**0.300**	0.353	0.310	**0.300**	19-24	2.553	**0.989**	1.229	1.226	1.308	1.094
8-10	0.301	0.301	**0.300**	0.302	0.303	**0.300**	20-13	1.049	1.068	0.993	0.964	0.873	**0.764**
9-7	**0.300**	**0.300**	**0.300**	**0.300**	0.312	**0.300**	20-16	0.980	0.995	0.951	0.887	0.917	**0.788**
10-12	**0.300**	0.336	**0.300**	0.301	0.312	**0.300**	21-18	**1.097**	23.416	5.006	1.806	2.084	2.172
11-9	**0.300**	**0.300**	0.301	0.303	0.302	**0.300**	21-20	**0.917**	2.416	2.442	1.191	1.383	1.403
12-14	**0.300**	0.302	**0.300**	0.304	0.301	**0.300**	21-24	2.697	1.167	1.327	1.260	1.340	**1.137**
12-21	0.488	0.309	0.364	0.382	0.333	**0.300**	22-11	0.831	0.947	0.941	1.002	0.890	**0.718**
13-11	**0.300**	**0.300**	**0.300**	0.339	0.301	**0.300**	22-14	**0.721**	0.941	0.876	0.886	0.858	0.745
13-21	0.379	0.301	**0.300**	0.302	0.301	0.329	23-18	**0.976**	23.157	4.771	1.696	1.961	1.994
14-16	**0.300**	0.302	**0.300**	0.303	0.302	**0.300**	23-20	**0.797**	2.157	2.206	1.082	1.260	1.225
14-19	0.607	0.374	0.341	0.379	0.306	**0.300**	23-22	2.859	1.820	2.831	**1.775**	2.388	1.892
15-13	**0.300**	**0.300**	0.301	0.301	0.311	**0.300**	24-5	**0.503**	0.879	0.889	0.745	0.741	0.694
15-19	0.538	**0.300**	**0.300**	0.301	0.360	0.324	24-8	**0.594**	0.867	0.739	0.781	0.728	0.689

The bold digits represent the minimum CTI value.

Table 10. CTI of P/B DOCRs-VROCRs pairs for 9-bus network.

DOCRs	VROCR1						VROCR2						VROCR3						VROCR4					
	GA	PSO	CSA	HSA	GA-NLP	HSA-NLP	GA	PSO	CSA	HSA	GA-NLP	HSA-BB	GA	PSO	CSA	HSA	GA-NLP	HSA-NLP	GA	PSO	CSA	HSA	GA-NLP	HSA-BB
1	0.335	**0.301**	0.310	0.305	0.483	0.321	2.852	2.572	2.701	2.770	2.637	**2.176**	2.595	2.262	2.193	1.943	2.243	**1.769**	2.486	2.786	2.806	2.648	2.556	**2.072**
2	5.052	5.113	4.820	4.796	5.142	**3.963**	7.003	6.529	6.722	6.807	6.383	**5.283**	3.832	3.470	3.393	3.005	3.326	**2.638**	5.043	5.619	5.621	5.295	5.034	**4.098**
3	4.829	4.756	4.479	4.560	4.872	**3.786**	6.781	6.172	6.382	6.571	6.114	**5.106**	3.609	3.113	3.053	2.769	3.056	**2.460**	4.820	5.262	5.281	5.059	4.764	**3.921**
4	4.914	5.029	4.708	4.713	5.037	**3.855**	5.580	5.238	5.397	5.479	5.120	**4.211**	0.518	0.469	0.523	0.370	0.510	**0.344**	3.138	3.588	3.608	3.380	3.209	**2.578**
5	4.928	4.835	4.431	4.536	4.852	**3.809**	5.595	5.044	5.119	5.302	4.935	**4.166**	0.533	**0.300**	**0.300**	0.310	0.325	**0.300**	3.153	3.394	3.331	3.204	3.024	**2.532**
6	3.075	3.162	2.976	2.990	3.216	**2.398**	3.143	2.931	3.082	3.141	2.910	**2.347**	1.190	1.059	1.077	0.898	1.055	**0.754**	0.897	1.126	1.204	1.090	1.024	**0.757**
7	3.166	3.150	2.826	3.025	3.203	**2.393**	3.234	2.918	2.932	3.176	2.898	**2.343**	1.281	1.046	0.927	0.933	1.043	**0.750**	0.988	1.113	1.054	1.125	1.012	**0.752**
8	5.263	5.463	4.982	5.170	5.370	**4.219**	4.831	4.602	4.639	4.883	4.416	**3.739**	3.583	3.346	3.119	2.930	3.085	**2.529**	**0.300**	0.408	0.378	0.440	0.302	0.301
9	5.534	5.498	5.000	5.248	5.555	**4.264**	5.102	4.638	4.656	4.961	4.602	**3.784**	3.855	3.381	3.137	3.007	3.270	**2.573**	0.441	0.444	0.396	0.517	0.487	**0.346**
10	6.652	6.774	6.225	6.351	6.681	**5.201**	4.921	4.602	4.668	4.832	4.443	**3.716**	5.722	5.226	4.929	4.527	4.859	**3.915**	2.997	3.424	3.357	3.230	2.991	**2.466**
11	6.962	6.882	6.359	6.626	6.935	**5.380**	5.230	4.710	4.802	5.107	4.697	**3.895**	6.031	5.334	5.063	4.802	5.113	**4.094**	3.306	3.532	3.491	3.504	3.245	**2.645**
12	3.027	2.988	2.821	2.779	3.066	**2.365**	0.592	**0.435**	0.559	0.498	0.540	0.448	3.266	2.865	2.787	2.439	2.762	**2.210**	2.348	2.577	2.619	2.407	2.341	**1.915**
13	2.735	2.855	2.577	2.605	2.839	**2.217**	**0.300**	0.302	0.316	0.324	0.313	**0.300**	2.974	2.732	2.544	2.266	2.535	**2.062**	2.056	2.444	2.376	2.234	2.114	**1.767**
14	1.687	1.696	1.539	1.632	1.730	**1.301**	1.731	1.547	1.607	1.730	1.533	**1.268**	2.441	2.148	2.025	1.864	2.016	**1.595**	1.978	2.254	2.225	2.168	1.967	**1.599**
15	1.619	1.622	1.498	1.554	1.783	**1.325**	1.662	1.473	1.566	1.651	1.587	**1.292**	2.372	2.074	1.983	1.786	2.070	**1.619**	1.909	2.180	2.184	2.089	2.021	**1.623**
16	0.392	0.413	0.306	0.316	0.326	**0.300**	2.909	2.684	2.696	2.781	2.480	**2.155**	2.652	2.374	2.188	1.954	2.086	**1.748**	2.543	2.898	2.801	2.659	2.399	**2.051**
17	0.765	0.812	0.704	0.706	0.748	**0.591**	0.790	0.724	0.744	0.763	0.633	**0.572**	1.017	0.902	0.824	0.689	0.754	**0.633**	0.771	0.959	0.930	0.850	0.728	**0.635**
18	1.005	1.019	0.925	0.942	0.993	**0.733**	3.522	3.289	3.315	3.407	3.147	**2.588**	3.265	2.980	2.807	2.580	2.752	**2.181**	3.156	3.504	3.420	3.285	3.066	**2.484**
19	0.526	0.696	0.622	0.650	0.769	**0.539**	0.551	0.608	0.662	0.707	0.653	**0.520**	0.778	0.786	0.742	0.634	0.775	**0.581**	**0.533**	0.842	0.848	0.795	0.749	0.583
20	2.368	2.390	2.190	2.216	2.345	**1.789**	2.411	2.241	2.259	2.314	2.148	**1.756**	3.122	2.842	2.676	2.448	2.631	**2.083**	2.658	2.948	2.876	2.752	2.583	**2.086**
21	0.670	0.874	0.719	0.684	0.800	**0.582**	0.695	0.786	0.760	0.742	0.685	**0.563**	0.922	0.964	0.839	0.668	0.806	**0.624**	0.677	1.020	0.946	0.829	0.780	**0.626**
22	3.266	3.502	3.218	3.269	3.428	**2.635**	0.831	0.949	0.957	0.987	0.902	**0.718**	3.505	3.380	3.185	2.929	3.124	**2.480**	2.587	3.091	3.017	2.897	2.703	**2.185**
23	0.549	0.614	0.484	0.575	0.677	**0.404**	0.575	0.526	0.524	0.632	0.562	**0.385**	0.802	0.705	0.604	0.558	0.683	**0.446**	0.556	0.761	0.710	0.719	0.657	**0.448**
24	3.369	3.729	3.415	3.470	3.643	**2.787**	3.437	3.497	3.520	3.620	3.338	**2.736**	1.484	1.625	1.515	1.378	1.482	**1.144**	1.191	1.693	1.642	1.570	1.451	**1.146**

The bold digits represent the minimum CTI value.

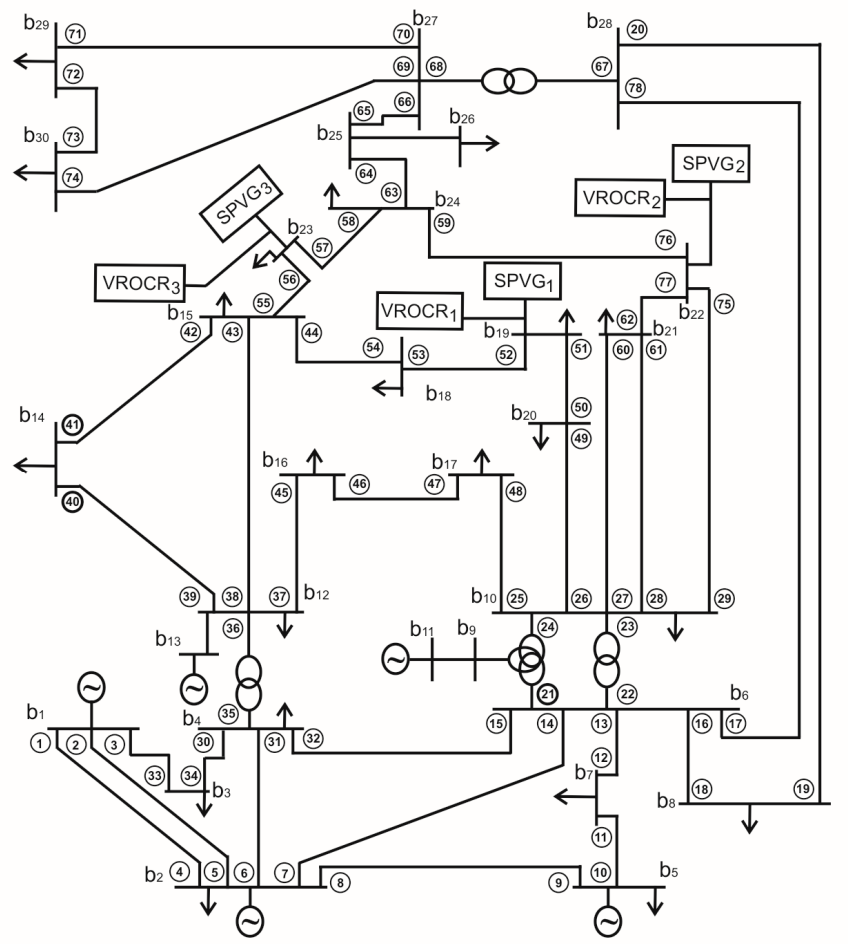

Figure 5. Diagram of three SPVGs connected IEEE 30 bus network.

Table 11 shows the results obtained by implementing all the methods for the IEEE 30-bus system. It comprises the OF values, numbers of violated coordination constraints, required numbers of iteration, and convergence time. The given OF value by HSA-BB, shown in Table 11, is the minimum compared to all other methods. It is also experienced that during the simulations of this complex system, sometimes hybrid GA-NLP does not converge even at a feasible solution and stops prematurely. Also, a violation of coordination constraints has been observed in GA, PSO, CSA, HSA, and GA-NLP, whereas there is no violation observed in the results of the proposed methods. The convergence of all algorithms is graphically illustrated in Figure 6. As seen in Table 11 and Figure 6, the numbers of iteration and convergence time are also lowest in the HSA-BB method as compared to GA, PSO, CSA, HSA, and GA-NLP methods. The simulation results confirm that HSA-BB gives better results compared to the remaining methods. However, the proposed HSA-BB algorithm has more parameters to be tuned as compared to the other methods. The tuning of the parameters is indeed a time consuming and tedious task. Also, the harmony memory size is bigger than the initially generated nest of the cuckoo search method. Therefore, it requires more memory to store the solutions.

Table 11. Comparative results for the IEEE 30-bus network.

Algorithm	OF (s)	Numbers of Violated CTI Constraints		Numbers of Iteration	Convergence Time (s)
		DOCRs-DOCRs Pairs	DOCRs-VROCRs Pairs		
GA	124.647	24	4	746	149.51
PSO	118.426	3	10	665	131.66
CSA	111.017	5	1	636	120.71
HSA	107.63	2	0	541	110.21
GA-NLP	102.019	1	1	162	47.54
HSA-BB	93.645	0	0	114	31.09

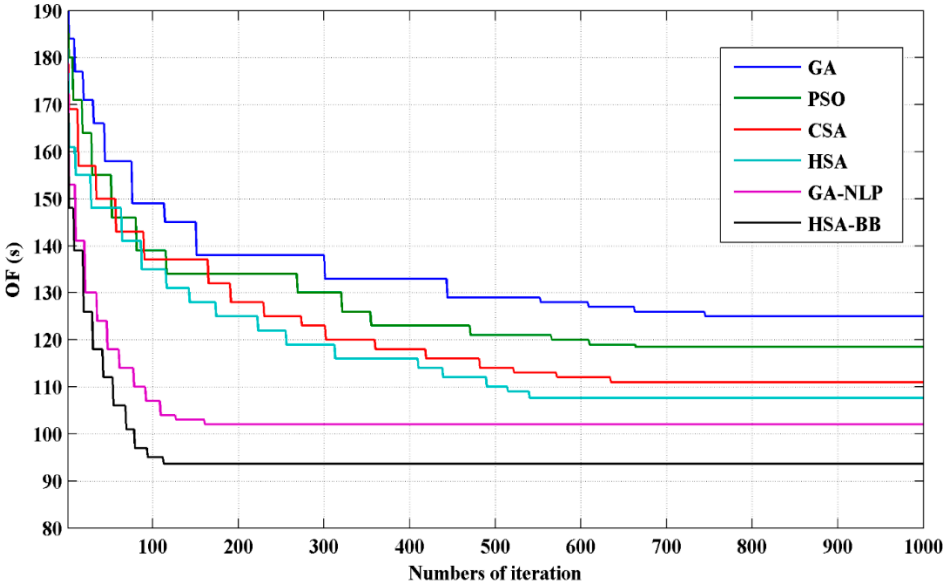

Figure 6. Convergence to the best objective function (OF) value for IEEE 30-bus network.

Furthermore, a comparative study of all the methods is performed, using descriptive and nonparametric statistical tests. Table 12 shows the results of a descriptive statistical study based on 50 runs. The lower value of standard deviation in the results of HSA-BB indicates that it gives the most predictable results in all 50 runs, compared to other methods. Additionally, because the mean and worst values are very near to the best value, quality results are obtained by HSA-BB.

Table 12. Descriptive statistical results based on 50 runs for IEEE 30-bus network.

Algorithm	OF (s)					
	Best	Worst	Mean	StdDev	Skewness	Kurtosis
GA	124.647	136.812	130.991	3.98	−0.08	−1.19
PSO	118.426	126.234	121.672	2.58	0.38	−1.35
CSA	111.017	114.872	113.140	1.29	−0.29	−1.20
HSA	107.63	110.937	108.813	1.13	0.39	−1.33
GA–NLP	102.019	103.900	102.937	0.772	0.05	−1.51
HSA–BB	93.645	94.096	93.878	0.205	−0.06	−1.94

Moreover, paired *t*-test and Wilcoxon signed-rank tests are widely used to determine the significant difference in the behavior and superiority of algorithms. However, the paired *t*-test is a parametric test and needs to be certain that the essential conditions are satisfied, i.e., independence, normality [48,49]. The condition of independence is fulfilled because 50 samples of the OF are obtained by 50 simulations of all algorithms with randomly produced initial seeds. Furthermore, samples from different runs were normal when their behavior assisted a normal or Gauss distribution.

The normality of the data is initially examined by the skewness and kurtosis. Skewness and kurtosis are needed to calculate the frequency distribution of data. Skewness helps to recognize the right and left tails of frequency distribution from a central value, while kurtosis gives an idea about the shape and nature of hump of a frequency distribution. The data can be said to be normally distributed when the skewness and kurtosis are equal to 0 and 3, respectively [50]. As seen in Table 12, the normal distribution is not verified from the results of skewness and kurtosis obtained by 50 runs of each algorithm. Hence, the statistical normality tests are further performed by using Anderson–Darling and Kolmogorov–Smirnov tests [48,49]. All the tests determine the *p*-value, which shows the variation of the sample of results concerning the normal shape. The *p*-value is less than the level of significance ($\alpha = 0.05$), indicating the rejections of normality. The results of *p*-values for all the algorithms by using normality tests are provided in Table 13. From Table 13, it is noted that both tests indicate that none of the outputs of the algorithms give perfect Gaussian distribution. Hence, it is justified to employ a nonparametric test, neglecting the parametric one.

Table 13. Comparative results of normality tests of all the algorithms.

Algorithm	*p*-Value	
	Anderson-Darling	Kolmogorov-Smirnov
GA	0.017	0.045
PSO	0.005	0.010
CSA	0.005	0.010
HSA	0.005	0.010
GA-NLP	0.005	0.010
HSA-BB	0.005	0.010

In this study, the effectiveness of the proposed hybrid algorithm over other algorithms is substantiated using Wilcoxon signed-rank test [48], which is a nonparametric test. In this test, a null hypothesis states that the behavior of algorithms which are compared to each other is similar, whereas an alternative hypothesis states the opposite. If the *p*-value for the null hypothesis is below the significant level ($\alpha = 0.05$), this hypothesis is rejected. The sum of rankings and *p*-value obtained in each comparison of algorithms is given in Table 14. From Table 14, it is seen that the *p*-value, when compared to HSA-BB with other algorithms, is below 0.05 and confirmed that the HSA-BB behaves differently compared to the remaining algorithms. In Table 14, R^+ is the sum of ranks for the data sets on which the first algorithm outperforms the second, and R^- is the sum of ranks for the opposite. From Table 14, it is seen that R^- is higher in all the comparison of other algorithms with HSA-BB. From the results of the Wilcoxon test, it is deduced that the proposed HSA-BB outperforms the GA, PSO, CSA, HSA, and GA-NLP algorithms with a significant level of 0.05.

Table 14. Comparative results of the Wilcoxon test of all the algorithms.

Comparison of Algorithms	R^+	R^-	*p*-Value
GA vs. HSA-BB	0	50	0.000
PSO vs. HSA-BB	0	50	0.000
CSA vs. HSA-BB	0	50	0.000
HSA vs. HSA-BB	0	50	0.000
GA-NLP vs. HSA-BB	0	50	0.000

5. Conclusions

This study presents a DOCR- and VROCR-based combined protection scheme. In this scheme, the VROCRs are used to operate for a low fault current on SPVG side protection, and DOCRs are implemented to sense a high fault current on grid side protection. This protection methodology provides

better fault detection for low fault current contributed by SPVG, and high fault current contributed by the grid. It also avoids unwanted isolation of SPVG in the case of short-term disturbances.

A hybrid HSA-BB method is employed to resolve the unique challenge of optimal coordination of DOCRs-DOCRs and DOCRs-VROCRs on three different SPVG-connected networks. The BB methodology is used in the improvisation stage of HSA. The BB method is also modified to dynamically adjust the gap between upper and lower bands with generation numbers so that it helps HSA in both exploration and exploitation.

For evaluating the capability of the proposed method in solving the relay coordination problem, the obtained results are compared with other well-established methods (GA, PSO, CSA, HSA, and GA-NLP). Outcomes of the comparative analysis validate that a significant reduction in the total operating time of relays is obtained using hybrid HSA-BB without violating the constraints compared to the other methods. In addition, the hybrid HSA-BB method takes minimum iteration to reach the best optimum solution, which reveals that the proposed method is also better in convergence performance. From the descriptive statistical test, it is found that the proposed method gives consistent solutions for different runs, which shows the capability of the proposed method in providing a better-quality solution. Furthermore, the results of nonparametric tests verify the significant difference in behavior as well as the superiority of the hybrid HSA-BB method compared to the other employed methods.

Author Contributions: Conceptualization, V.N.R., K.S.P.; Methodology, V.N.R., K.S.P.; Writing—Original Draft Preparation, V.N.R.; Writing-Review & Editing, Z.W.G., J.H.; Supervision, K.S.P., Z.W.G.; Funding Acquisition, Z.W.G., J.H. All authors have read and agreed to the published version of the manuscript.

Funding: This research was supported by the Energy Cloud R&D Program through the National Research Foundation of Korea (NRF) funded by the Ministry of Science, ICT (2019M3F2A1073164).

Conflicts of Interest: The authors declare no conflict of interest.

References

1. Hernández, J.; De la Cruz, J.; Ogayar, B. Electrical protection for the grid-interconnection of photovoltaic-distributed generation. *Electr. Power Syst. Res.* **2012**, *89*, 85–99. [CrossRef]
2. Geem, Z.W. Size optimization for a hybrid photovoltaic–wind energy system. *Int. J. Electr. Power Energy Syst.* **2012**, *42*, 448–451. [CrossRef]
3. Shin, H.; Geem, Z.W. Optimal design of a residential photovoltaic renewable system in South Korea. *Appl. Sci.* **2019**, *9*, 1138. [CrossRef]
4. Cagnano, A.; De Tuglie, E.; Mancarella, P. Microgrids: Overview and guidelines for practical implementations and operation. *Appl. Energy* **2020**, *258*, 114039. [CrossRef]
5. Amraee, T. Coordination of directional overcurrent relays using seeker algorithm. *IEEE Trans. Power Deliv.* **2012**, *27*, 1415–1422. [CrossRef]
6. Bedekar, P.P.; Bhide, S.R. Optimum coordination of directional overcurrent relays using the hybrid GA-NLP approach. *IEEE Trans. Power Deliv.* **2011**, *26*, 109–119. [CrossRef]
7. Noghabi, A.S.; Sadeh, J.; Mashhadi, H.R. Considering different network topologies in optimal overcurrent relay coordination using a hybrid GA. *IEEE Trans. Power Deliv.* **2009**, *24*, 1857–1863. [CrossRef]
8. Rajput, V.N.; Pandya, K.S. Coordination of directional overcurrent relays in the interconnected power systems using effective tuning of harmony search algorithm. *Sustain. Comput. Inform. Syst.* **2017**, *15*, 1–15. [CrossRef]
9. Kida, A.A.; Labrador Rivas, A.E.; Gallego, L.A. An improved simulated annealing–linear programming hybrid algorithm applied to the optimal coordination of directional overcurrent relays. *Electr. Power Syst. Res.* **2020**, *181*, 106197. [CrossRef]
10. Srinivas, S.T.P.; Shanti Swarup, K. Application of improved invasive weed optimization technique for optimally setting directional overcurrent relays in power systems. *Appl. Soft Comput.* **2019**, *79*, 1–13. [CrossRef]
11. Wadood, A.; Gholami Farkoush, S.; Khurshaid, T.; Kim, C.-H.; Yu, J.; Geem, Z.W.; Rhee, S.-B. An optimized protection coordination scheme for the optimal coordination of overcurrent relays using a nature-inspired root tree algorithm. *Appl. Sci.* **2018**, *8*, 1664. [CrossRef]
12. Gaonkar, D. *Distributed Generation*; IntechOpen: Rijeka, Croatia, 2010; pp. 289–310.

13. Dewadasa, M.; Ghosh, A.; Ledwich, G. Fold back current control and admittance protection scheme for a distribution network containing distributed generators. *IET Gener. Transm. Distrib.* **2010**, *4*, 952–962. [CrossRef]
14. Vieira, J.C.; Freitas, W.; Xu, W.; Morelato, A. Performance of frequency relays for distributed generation protection. *IEEE Trans. Power Deliv.* **2006**, *21*, 1120–1127. [CrossRef]
15. Ustun, T.S.; Ozansoy, C.; Ustun, A. Fault current coefficient and time delay assignment for microgrid protection system with central protection unit. *IEEE Trans. Power Syst.* **2013**, *28*, 598–606. [CrossRef]
16. Chabanloo, R.; Abyaneh, H.A.; Agheli, A.; Rastegar, H. Overcurrent relays coordination considering transient behaviour of fault current limiter and distributed generation in distribution power network. *IET Gener. Transm. Distrib.* **2011**, *5*, 903–911. [CrossRef]
17. El-Khattam, W.; Sidhu, T.S. Restoration of directional overcurrent relay coordination in distributed generation systems utilizing fault current limiter. *IEEE Trans. Power Deliv.* **2008**, *23*, 576–585. [CrossRef]
18. Farzinfar, M.; Jazaeri, M. A novel methodology in optimal setting of directional fault current limiter and protection of the MG. *Int. J. Electr. Power Energy Syst.* **2020**, *116*, 105564. [CrossRef]
19. Mirsaeidi, S.; Said, D.M.; Mustafa, M.W.; Habibuddin, M.H.; Ghaffari, K. An analytical literature review of the available techniques for the protection of micro-grids. *Int. J. Electr. Power Energy Syst.* **2014**, *58*, 300–306. [CrossRef]
20. Al-Nasseri, H.; Redfern, M. Harmonics content based protection scheme for micro-grids dominated by solid state converters. In Proceedings of the 12th International Middle-East Power System Conference, Aswan, Egypt, 12–15 March 2008; pp. 50–56. [CrossRef]
21. Brahma, S.M.; Girgis, A.A. Development of adaptive protection scheme for distribution systems with high penetration of distributed generation. *IEEE Trans. Power Deliv.* **2004**, *19*, 56–63. [CrossRef]
22. Lien, K.-Y.; Bui, D.M.; Chen, S.-L.; Zhao, W.-X.; Chang, Y.-R.; Lee, Y.-D.; Jiang, J.-L. A novel fault protection system using communication-assisted digital relays for AC microgrids having a multiple grounding system. *Int. J. Electr. Power Energy Syst.* **2016**, *78*, 600–625. [CrossRef]
23. Sharma, N.K.; Samantaray, S.R. PMU assisted integrated impedance angle-based microgrid protection scheme. *IEEE Trans. Power Deliv.* **2020**, *35*, 183–193. [CrossRef]
24. Habib, H.F.; Lashway, C.R.; Mohammed, O.A. A review of communication failure impacts on adaptive microgrid protection schemes and the use of energy storage as a contingency. *IEEE Trans. Ind. Appl.* **2018**, *54*, 1194–1207. [CrossRef]
25. Nsengiyaremye, J.; Pal, B.C.; Begovic, M.M. Microgrid protection using low-cost communication systems. *IEEE Trans. Power Deliv.* **2019**. [CrossRef]
26. Sortomme, E.; Ren, J.; Venkata, S.S. A differential zone protection scheme for microgrids. In Proceedings of the IEEE Power & Energy Society General Meeting, Vancouver, BC, Canada, 21–25 July 2013; pp. 1–5. [CrossRef]
27. Jayawarna, N.; Barnes, M. Central storage unit response requirement in 'Good Citizen'microgrid. In Proceedings of the 2009 13th European Conference on Power Electronics and Applications, Barcelona, Spain, 8–10 September 2009; pp. 1–10.
28. van Overbeeke, F. Fault current source to ensure the fault level in inverter dominated networks. In Proceedings of the CIRED 2009—The 20th International Conference and Exhibition on Electricity Distribution—Part 2, Prague, Czech Republic, 8–11 June 2009; pp. 1–13.
29. El-Naily, N.; Saad, S.M.; Hussein, T.; Mohamed, F.A. A novel constraint and non-standard characteristics for optimal over-current relays coordination to enhance microgrid protection scheme. *IIET Gener. Transm. Distrib.* **2019**, *13*, 780–793. [CrossRef]
30. Kılıçkıran, H.C.; Akdemir, H.; Şengör, İ.; Kekezoğlu, B.; Paterakis, N.G. A non-standard characteristic based protection scheme for distribution networks. *Energies* **2018**, *11*, 1241. [CrossRef]
31. Ehrenberger, J.; Švec, J. Directional overcurrent relays coordination problems in distributed generation systems. *Energies* **2017**, *10*, 1452. [CrossRef]
32. Kiliçkiran, H.C.; Şengör, İ.; Akdemir, H.; Kekezoğlu, B.; Erdinç, O.; Paterakis, N.G. Power system protection with digital overcurrent relays: A review of non-standard characteristics. *Electr. Power Syst. Res.* **2018**, *164*, 89–102. [CrossRef]

33. Banu, I.V.; Istrate, M. Study on three-phase photovoltaic systems under grid faults. In Proceedings of the 2014 International Conference and Exposition on Electrical and Power Engineering (EPE), Iasi, Romania, 16–18 October 2014; pp. 1132–1137. [CrossRef]
34. Falvo, M.C.; Capparella, S. Safety issues in PV systems: Design choices for a secure fault detection and for preventing fire risk. *Case Stud. Fire Saf.* **2015**, *3*, 1–16. [CrossRef]
35. Alsharif, M.H.; Yahya, K.; Geem, Z.W. Strategic market growth and policy recommendations for sustainable solar energy deployment in South Korea. *J. Electr. Eng. Technol.* **2020**, *15*, 803–815. [CrossRef]
36. Voltage Restrained Overcurrent Relay and Protection Assemblies. Available online: https://new.abb.com/substation-automation/products/protection-control/modular-relays-and-accessories/measuring-relays/limited-measuring-relays/rxisk (accessed on 12 April 2017).
37. Ventruella, D.; Steciuk, P. A second look at generator 51-V relays. *IEEE Trans. Ind. Appl.* **1997**, *33*, 848–856. [CrossRef]
38. Geem, Z.W.; Kim, J.H.; Loganathan, G.V. A new heuristic optimization algorithm: Harmony search. *Simulation* **2001**, *76*, 60–68. [CrossRef]
39. Fesanghary, M.; Mahdavi, M.; Minary-Jolandan, M.; Alizadeh, Y. Hybridizing harmony search algorithm with sequential quadratic programming for engineering optimization problems. *Comput. Methods Appl. Mech. Eng.* **2008**, *197*, 3080–3091. [CrossRef]
40. Lee, K.S.; Geem, Z.W. A new meta-heuristic algorithm for continuous engineering optimization: Harmony search theory and practice. *Comput. Methods Appl. Mech. Eng.* **2005**, *194*, 3902–3933. [CrossRef]
41. Geem, Z.W.; Yoon, Y. Harmony search optimization of renewable energy charging with energy storage system. *Int. J. Electr. Power Energy Syst.* **2017**, *86*, 120–126. [CrossRef]
42. Thakkar, A.; Kotecha, K. A new Bollinger Band based energy efficient routing for clustered wireless sensor network. *Appl. Soft Comput.* **2015**, *32*, 144–153. [CrossRef]
43. Zhu, Q.; Tang, X.; Li, Y.; Yeboah, M.O. An improved differential-based harmony search algorithm with linear dynamic domain. *Knowl. Based Syst.* **2020**, *187*, 104809. [CrossRef]
44. Lan, H.; Liao, Z.-m.; Yuan, T.-g.; Zhu, F. Calculation of PV power station access. *Energy Procedia* **2012**, *17*, 1452–1459. [CrossRef]
45. Mandal, A. Design & Estimation of 1 MW Utility Scale Solar PV Power Plant: Technical & Financial. Available online: http://www.academia.edu/5449881 (accessed on 21 February 2017).
46. Teodorescu, R.; Liserre, M.; Rodriguez, P. *Grid Converters for Photovoltaic and Wind Power Systems*; John Wiley & Sons: Hoboken, NJ, USA, 2010. [CrossRef]
47. Rajput, V.N.; Pandya, K.S. On 8-bus test system for solving challenges in relay coordination. In Proceedings of the 2016 IEEE 6th International Conference on Power Systems (ICPS), New Delhi, India, 4–6 March 2016; pp. 1–5. [CrossRef]
48. García, S.; Molina, D.; Lozano, M.; Herrera, F. A study on the use of non-parametric tests for analyzing the evolutionary algorithms' behaviour: A case study on the CEC'2005 special session on real parameter optimization. *J. Heuristics* **2009**, *15*, 617. [CrossRef]
49. Trawiński, B.; Smętek, M.; Telec, Z.; Lasota, T. Nonparametric statistical analysis for multiple comparison of machine learning regression algorithms. *Int. J. Appl. Math. Comput. Sci.* **2012**, *22*, 867–881. [CrossRef]
50. Fentaw, F.; Melesse, A.M.; Hailu, D.; Nigussie, A. Precipitation and streamflow variability in Tekeze River basin, Ethiopia. In *Extreme Hydrology and Climate Variability*; Melesse, A.M., Abtew, W., Senay, G., Eds.; Elsevier: Amsterdam, The Netherlands, 2019; pp. 103–121. [CrossRef]